Desalination and Water Treatment
www.deswater.com
doi: 10.5004/dwt.2020.25662

190 (2020) 193–202
June

The adsorption properties of 2,4-DCP on biochar derived from chitosan in aqueous solution

Jian Wu[a], Dajun Ren[a,b,*], Shuqin Zhang[a,b], Wenting Liu[a], Xiaoqin Zhang[a,b], Xiangyi Gong[a,b]

[a]*College of Resource and Environmental Engineering, Wuhan University of Science and Technology, Wuhan, 430081, China, Tel. +86 027-68862029; Fax: +86 027-68862029; emails: dj_ren@163.com (D. Ren), wj_5412@163.com (J. Wu), 57791098@qq.com (S. Zhang), 1183111932@qq.com (W. Liu), friedchickenlg@126.com (X. Zhang), gongxiangyi@wust.edu.cn (X. Gong)*
[b]*Hubei Key Laboratory for Efficient Utilization and Agglomeration of Metallurgic Mineral Resources, Wuhan University of Science and Technology, Wuhan, Hubei 430081, China*

Received 9 August 2019; Accepted 6 February 2020

ABSTRACT

Organic pollutants in aqueous solutions may potentially be adsorbed on biochar. In this study, biochar was derived from the pyrolysis of chitosan at 800°C. The removal rate of 2,4-dichlorophenol (DCP) exceeded 80%. Investigations by Fourier transform infrared spectroscopy and Brunauer–Emmett–Teller indicated that the adsorption of organic pollutants on biochar tends to be a physical process. The optimized pH was 5. All three isotherm models involved (Freundlich, Koble–Corrigan, and Henry) could describe the adsorption process of 2,4-DCP well on chitosan-biochar, which was non-uniform surface adsorption in a diluted solution. The adsorption was an endothermic process. It took 40 min to reach the adsorption equilibrium, and kinetics of the Elovich equation and intraparticle diffusion (IPD) model indicated that the adsorption rate at the rapid adsorption stage was simultaneously controlled by surface diffusion and IPD and that at slow adsorption stage was controlled by surface diffusion. The ionic strengths suggested that electrostatic interaction was not the dominant mechanism during this process.

Keywords: Chitosan; Biochar; 2,4-Dichlorophenol; Adsorption

1. Introduction

Among all pollutants in aquatic ecosystems, phenols, especially the chlorinated ones, are considered as most severe pollutants as they are hazardous to organisms even at ppb levels [1]. 2,4-dichlorophenol (2,4-DCP) is an intermediate for the synthesis of various pesticides and fungicides and widely applied in the manufacturing of preservatives and certain methylphenol phenolic compounds commonly used in seed disinfection. Indeed, 2,4-DCP was listed as a priority control object by both the US Environmental Protection Agency and the China Environmental Monitoring Center [2,3]. Accumulation of 2,4-DCP in human body via food chain may threaten human health by changing the conformation of serum proteins and the microenvironment [4]. Hence, effective degradation of 2,4-DCP has become a hot topic globally. To date, methods for removal of 2,4-DCP are based on electrochemical oxidation process [5], photo-catalytic oxidation [6], zero-valent metal reduction [7], and/or adsorption [8].

Biochar, which can be commonly derived by pyrolysis of biomasses such as agricultural wastes (e.g., chicken manure [9], pig manure, sawdust [10]), and urban sludge [11]) has attracted great attention. Biochar is categorized by solubility, stability, aromatization, and carbon enrichment [12]. The constituent elements of biochar include carbon, hydrogen, oxygen, etc., and it is characterized by high carbon enrichment. In terms of microscopic structure,

* Corresponding author.

bio-carbon consists of closely packed, highly distorted aromatic ring sheets with chaotic structures [13], suggested by X-ray investigations. Therefore, biochar tends to have large specific surface area and high surface energy, making it an ideal candidate for the adsorbent. Zhang et al. [14] found that rice husks were one of the sustainable silica sources for hierarchical flower-like metal silicate, and three-dimensional (3D) hierarchical flower-like metals, which were prepared by using rice husks as a sustainable silicon source silicate, exhibited high catalytic activity and adsorption capacity. Liu et al. [15] found that high performance of phosphate-functionalized graphene oxide selectively adsorbed U(VI) from acidic solution, and it was a chemical absorption process. Liu et al. [16] found that amidoxime-functionalized hollow carbon spheres (C–HCN–AO) exhibited good absorption capacity, and the process was predominantly controlled by inner-sphere complexation. Indeed, biochar can be used to remove organic pollutants, including benzoquinone [17], toluene [18], and quinoline [19], from aqueous solutions. Sun et al. [20] found that the adsorption capacity of ACs, activated carbons with different oxidation degrees, towards phenols and resorcinol decreased with increasing oxidation degrees, and the chemical adsorption was not mainly dominant in the adsorption process. Oh et al. [21] applied a novel biochar-coated zero-valent iron [Fe(0)] to remove nitro explosives (2,4,6-trinitrotoluene and hexahydro-1,3,5-trinitro-1,3,5-triazine) and halogenated phenols (2,4-dibromophenol and 2,4-difluorophenol) from contaminated waters, and the removal of nitro explosives and halogenated phenols was significantly enhanced via sorption. It indicated that biomass could be used to synthesize a novel sorbent and catalyst for treating organic pollutants.

Seafood is a very popular food in China. More than 0.8 million tons of crabs and 1.2 million tons of crayfish are eaten each year in China. This would cause a lot of food waste. How to recycle it is a matter of great concern. The preparation of chitin and chitosan is a way to recycle these seafood food wastes [22].

In the present study, biochar was synthesized with chitosan as raw material at 800°C and characterized by Fourier transform infrared spectroscopy (FTIR), scanning electron microscope (SEM), and Brunauer–Emmett–Teller (BET). The removal capacity, potential adsorption mechanism, kinetics, adsorption isotherms, and thermodynamic properties involved in removal of 2,4-DCP were investigated.

2. Materials and methods

2.1. Preparation of chitosan-biochar

Chitosan in a quartz crucible was placed in a vacuum tube furnace, which was heated to 800°C, kept at 800°C for 4 h, and cooled to room temperature under nitrogen. The chitosan-biochar (CBC) obtained was then ground.

2.2. Batch equilibrium experiment

A solution with 100 mg/L 2,4-DCP was prepared. The pH value of the solution was adjusted to 3–10 using diluted HCl or NaOH, and CBC was added in to generate a solution with 2 g/L CBC. The products were centrifugated at 3,000 rpm for 10 min and then filtered by a 0.45 μm filter head. The concentrations of 2,4-DCP were measured by high-performance liquid chromatography (HPLC) to determine the optimized pH value. All experiments were repeated for three times. The adsorption capacities were calculated by [23]:

$$Q_e = \frac{V\left(C_0 - C_e\right)}{m} \tag{1}$$

The removal rates were calculated by:

$$R = 100\% \times \frac{\left(C_0 - C_e\right)}{C_0} \tag{2}$$

where Q_e (mg/g) is the adsorption capacity; C_0 is the initial solution concentration (mg/L); C_e (mg/L) is the equilibrium solution concentration; V is the solution volume (L); m (g) is the biochar mass.

2.3. Adsorption isotherms

The adsorption isotherms were determined by batch adsorptions at constant temperatures (298, 308, and 318 K), with mechanical shaking (–150 rpm), and in a contact time of 4 h. The initial concentrations of 2,4-DCP were 20–300 mg/L, which were prepared by diluting the stock solution. CBC was added to the 2,4-DCP solution at optimized pH values and the mixtures were centrifuged at 3,000 rpm and filtered by a 0.45 μm membrane for 2,4-DCP analysis by HPLC. All experiments were repeated for three times.

2.4. Adsorption kinetics

The solution with 100 mg/L 2,4-DCP was prepared. The pH value of the solution was adjusted to five using diluted HCl, and CBC was added in to generate a solution with 2 g/L CBC. At a constant temperature of 308 K, the solution oscillated at a speed of 150 rpm. The time was set to be 5–90 min, respectively. After that, the supernatant was filtered by a 0.45 μm membrane, and the concentration of 2,4-DCP was measured by HPLC for calculating the adsorption capacity and the removal rate. All experiments were repeated for three times.

2.5. Effect of ionic strength on adsorption

The solutions, with 100 mg/L 2,4-DCP, varied the concentrations of NaCl in 0.01–0.1 mol/L. The pH value of the solution was adjusted to five using diluted HCl, and CBC was added in to generate a solution with 2 g/L CBC. At a constant temperature of 308 K, the solution oscillated at a speed of 150 rpm. The time was set to be 2 h. After that, the supernatant was filtered by a 0.45 μm membrane, and the concentration of 2,4-DCP was measured by HPLC for calculating the adsorption capacity and the removal rate.

2.6. Sample characterization

CBC was mixed with monocrystal KBr (CAS:7758–02–3, SP grade, Aladdin, China) in a 1/100 m/m ratio and then

tableted. The tablets were analyzed by an FTIR spectrophotometer (VERTEX 70, Bruker, Germany) in wave number of 4,000–400 cm^{-1} to investigate the surface functional groups. The Zeta potential was measured by Zeta potential measurement with Submicron particle size analyzer. The microstructure of biochar was investigated using SEM. Before that, the biochar was coated by a gold-palladium film. Isotherm linear, analyzed by the TriStar II 3 flex type-specific surface area analyzer, was obtained with 77 K N_2 as the adsorption medium, and the specific surface area was calculated by the BET method.

3. Results and discussion

3.1. Biochar characterization

3.1.1. Fourier transform infrared spectroscopy

The FTIR spectra obtained using the Thermo Scientific (America) OMNIC software are shown in Fig. 1. As observed, the biochar contains aliphatic nitro compounds and alcohol functional groups before and after adsorption, respectively. The 1,563 cm^{-1} peak was assigned to strong absorptions of the nitro compounds [24]. The 3,433 cm^{-1} peak was attributed the free –OH stretching vibration [25], indicating that biochar contained a certain amount of hydroxyl groups, and the asymmetry of the peak shape was due to the presence of hydrogen bonds. The 1,650 cm^{-1} peak was put down to the C=O stretching vibration [26]. The 1,108 cm^{-1} peak was ascribed to the C–O stretching vibration of a secondary alcohol. It was deduced that the nitro groups were generated by recombination of amine groups and oxygen atoms in the molecular chain of the chitosan during pyrolysis, while alcohol functional groups were mainly derived from recombination of oxygen atoms in chitosan during pyrolysis and their intrinsic ones. In particular, the FTIR spectra indicated no significant difference before and after adsorption. Analysis by the Thermo Scientific OMNIC software showed no changes in either the surface chemical groups or chemical bonds after adsorption.

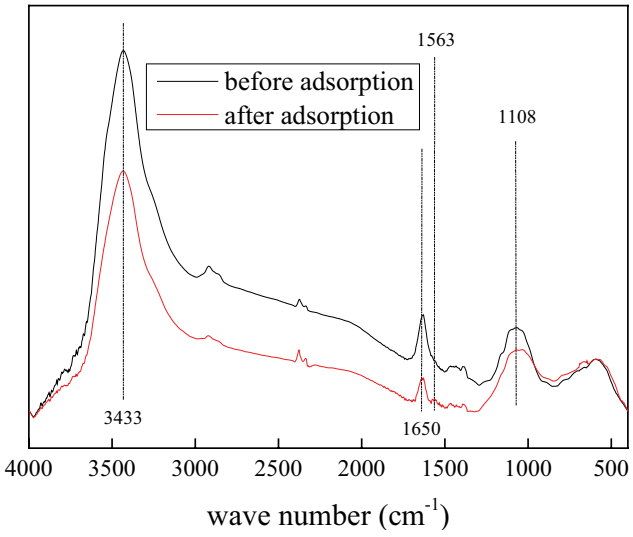

Fig. 1. FTIR spectra of Biochar.

3.1.2. Scanning electron microscopy

The SEM images of CBC are shown in Fig. 2. As observed, CBC was a bulky substance with a layered structure. Melting between the biochar layers was observed and it could be attributed to sintering, which might be caused by over-heating. However, biochar was not fully bonded together and significant interlayer gaps were observed. As a result, a new internal channel of biochar was presented, resulting in enhancing adsorption capacity. Additionally, branch-like extensions were commonly observed on biochar surfaces and these extensions might facilitate the capture of molecular adsorbents by increasing the possibility of contacting between active sites and adsorbents.

3.1.3. Brunauer–Emmett–Teller

The specific surface area of CBC, calculated by the BET method, was 60.7185 m^2/g, and the N_2 adsorption–desorption isotherm of CBC is shown in Fig. 3. According to the IUPAC classification of isotherms, this isotherm was an IUPAC type II one, which reflected typical physical adsorption on non-porous or macroporous adsorbents. Due to the strong interaction of adsorbates on the surface, the adsorbate density increased rapidly at low relative pressures and the curve was convex. The inflection point of isotherm appeared in the vicinity of single-layer adsorption. As the relative pressure increased, multi-layer adsorption increased. Upon reaching the saturated vapor pressure, the adsorption layer was infinite and it was highly difficult to determine the accurate adsorption equilibrium.

The Barret–Joyner–Halenda theory (BJH) pore size distribution of CBC is shown in Fig. 4. The pore diameter of CBC was mainly distributed in 2–10 nm. The average pore diameter was 4.96 nm. The total pore volume was 0.137 cm^3/g. In particular, the ratio of micropore pore volume to total pore volume was about 15.25%, indicating that the micropore amount of CBC was of little.

3.2. Effect of pH value

The pH value is an important factor in adsorption as it affects the surface charge of adsorbents, the degree of ionization, and the initial form of 2,4-DCP in the solution [27]. The effect of the pH value on the adsorption of 2,4-DCP by CBC is shown in Fig. 5. As observed, the removal rate of 2,4-DCP decreased as the pH value increased. At pH values no larger than 5, the adsorption capacity and removal rate remain constant; at pH values larger than 5, the adsorption capacity and the removal rate tended to drop rapidly to a saturated level. Therefore, the optimized pH value was 5 in this study. Similar acidic conditions were suitable for biochar produced from metal-nitrate modified activated carbon [28]. This might be attributed to the effects of pH values on the properties of 2,4-DCP and adsorbents.

2,4-DCP is a hydrophobic organic substance. In response to changes in pH value in solution, 2,4-DCP may be exposed

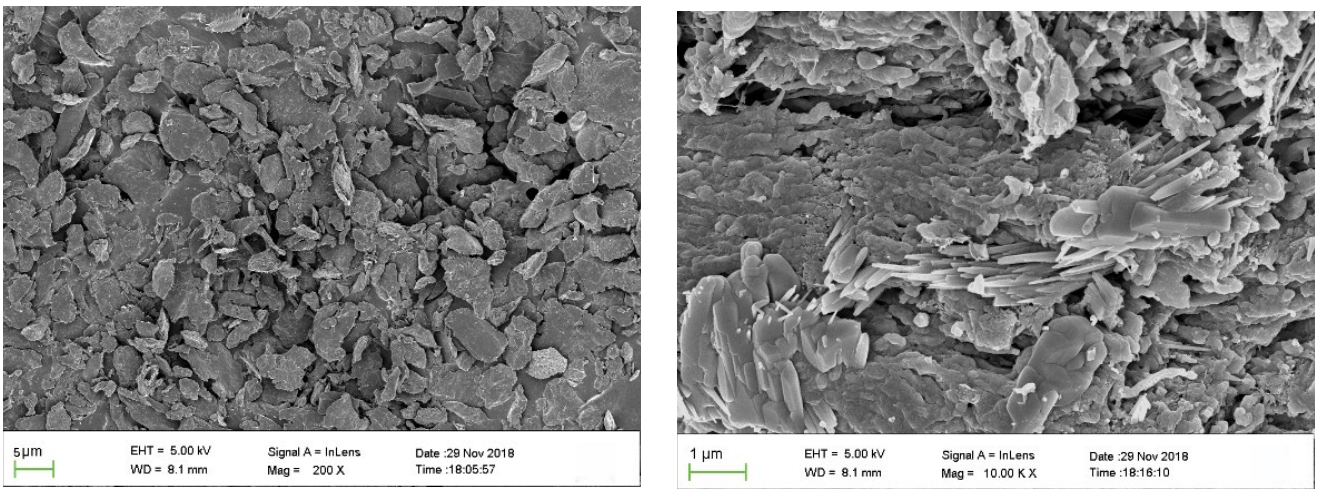

Fig. 2. SEM images of CBC.

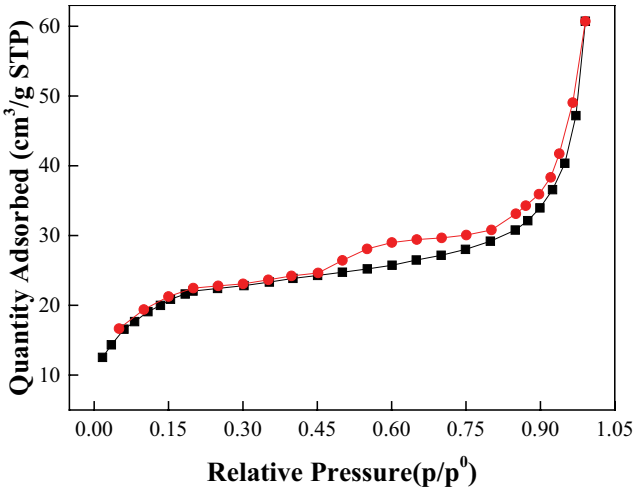

Fig. 3. The N_2 adsorption–desorption isotherm of CBC.

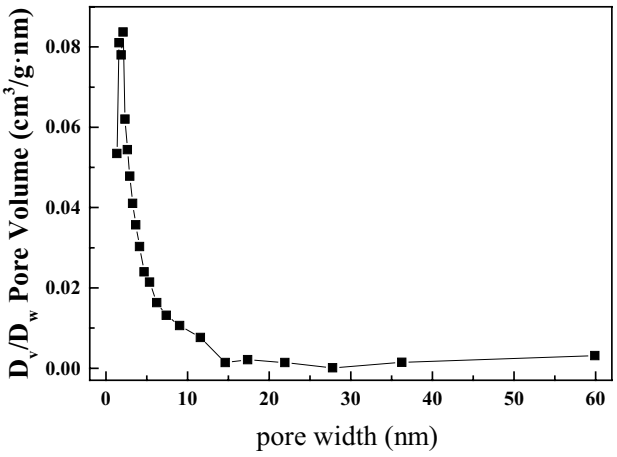

Fig. 4. The BJH pore size distribution of CBC.

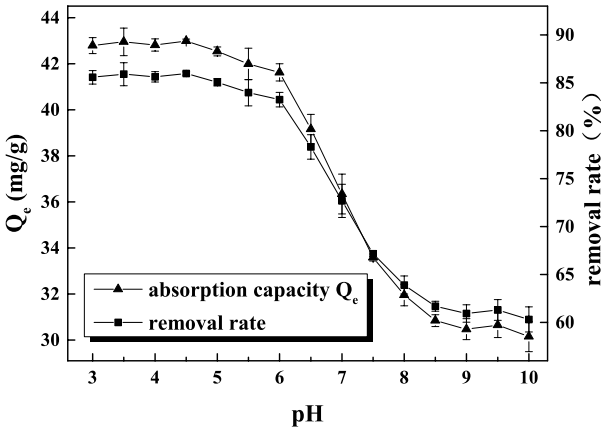

Fig. 5. Effect of initial pH value on 2,4-DCP removal.

to protonation and/or dephosphorization. The dissociation process and equilibrium constant are [29]:

$$2,4\text{-DCP} \leftrightarrow 2,4\text{-DCP}^- + H^+ \qquad pKa = 7.85 \qquad (3)$$

The morphologies of 2,4-DCP at different pH values were obtained at room temperature (Fig. 6). As observed, 2,4-DCP is mainly in molecular form and at ionic state under acidic and alkaline conditions, respectively. Additionally, the solubility of 2,4-DCP in aqueous solution was maximized at anionic state, and bonds of 2,4-DCP and water molecules tended to be strong, resulting in a decrease in hydrophobicity and possibility of binding with CBC active sites. Hence, adsorption of 2,4-DCP was more favorable in molecular form than that at the ionic state.

Fig. 7 shows the zeta potential of CBC under different pH conditions. According to Fig. 7, pHzpc value of CBC was 5.86, and the adsorbent surface was electrically neutral at the pHzpc point.

At pH levels below the isoelectric point (pHpzc) of CBC, the surface of CBC was positively charged, and the molecular form was dominated by the 2,4-DCP structure. Electrostatic repulsion between adsorbent and adsorbate was negligible in this case. The adsorption was driven by van der Waals forces. Therefore, the effect of pH on the adsorption was

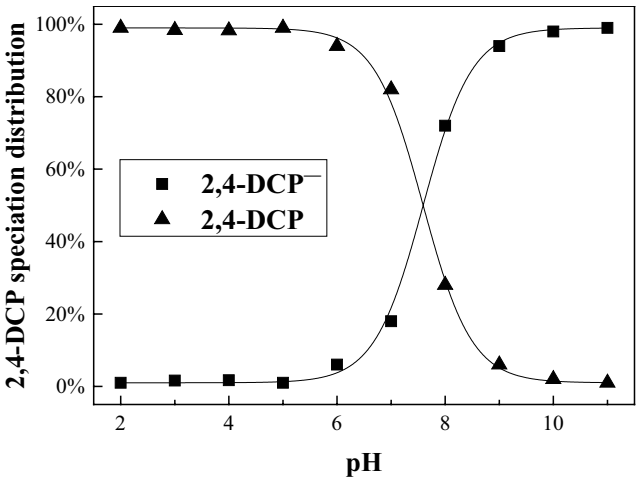

Fig. 6. Speciation distributions of 2,4-DCP in aqueous solutions.

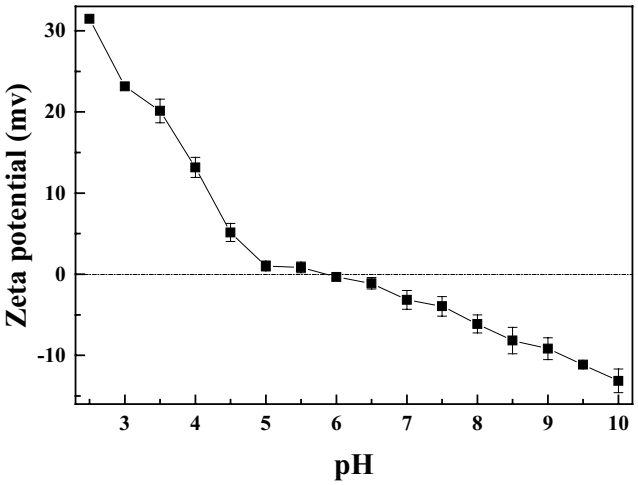

Fig. 7. Values of the zeta potential under different pH conditions.

minimized under acidic conditions from the point of view of both adsorbent and adsorbate.

At pH levels above the pHpzc of CBC, the surface of the CBC was negatively charged and the state-dominated the 2,4-DCP structure, whose surface was also negatively charged. Therefore, significant electrostatic repulsion was observed between adsorbates and adsorbates with active sites on CBC surface. As a result, adsorption of 2,4-DCP to CBC was hindered. Meanwhile, the adsorbent surface would carry more negative charges as the pH value increases, and the dissociation degree of 2,4-DCP would be greater, resulting in the increase of electrostatic repulsion and the degradation of adsorption. Once the pH value increased to a critical level, the degree of negative charges of the two systems was saturated, as well as the adsorption capacity. The adsorption processes at different pH levels are shown in Fig. 8.

3.3. Kinetics and adsorption isotherms

3.3.1. Adsorption isotherms

The relationship between equilibrium concentrations of 2,4-DCP and adsorption capacities of CBC is shown in Fig. 9. As observed, the adsorption capacity increased as the initial concentration of 2,4-DCP increased. Once the concentration of 2,4-DCP reached the equilibrium level, the adsorption capacity remained unchanged. This may be attributed to the fact that the density of active sites, which could bind 2,4-DCP successfully, tends to be low at low concentrations of 2,4-DCP. Meanwhile, the adsorption capacity increased with the increase of temperature at consistent initial concentration. Hence, it could be deduced that the adsorption was favorable at high temperatures and the adsorption of 2,4-DCP by CBC was an endothermic process.

In this study, models based on Freundlich, Koble–Corrigan, and Henry equations were used to fit the experimental data. The Freundlich equation is an empirical formula expressed in an exponential adsorption isotherm [30,31]:

$$Q_e = K_F C_e^{\frac{1}{n}} \tag{4}$$

$$\log\left(Q_e\right) = \log K_F + \frac{1}{n}\log C_e \tag{5}$$

where K_F is a parameter of Freundlich adsorption capacity; n is an empirical parameter that describes the adsorption strength, which is directly related to the heterogeneity of the adsorbents.

The Koble–Corrigan equation is a combination of the Freundlich model and the Langmuir model. Its nonlinear form was expressed as [32]:

$$Q_e = \frac{AC_e^n}{1 + BC_e^n} \tag{6}$$

where A, B, and n are the Koble–Corrigan parameters. This model is valid when $1/n < 1$.

The Henry model is suitable for the adsorption process carried out in dilute solutions. Its linear form was expressed as:

$$Q_e = A + KC_e \tag{7}$$

where A and K are the Henry model parameters.

The parameters of the three model were evaluated and summarized in Table 1. Fig. 10 shows that the value of K_F of the Freundlich model increased with the increase of temperature. As observed, the interaction between adsorbate and adsorbent was enhanced by high temperatures. The value of $1/n$ was less than 1, indicating that the adsorption was readily possible. The correlation coefficient R^2, fitted by the Freundlich equation, was greater than 0.98 and the error values were negligible. Therefore, the Freundlich equation could be used to describe the adsorption behavior.

As shown in Fig. 11, parameters A and B in Koble–Corrigan model remained constant as temperature increased. The value of n varied significantly from l, indicating that the Koble–Corrigan model did not approach the Langmuir model. The correlation coefficient R^2 exceeded 0.97, and the error value was negligible. The Koble–Corrigan model could describe the adsorption of 2,4-DCP on CBC, while the Henry

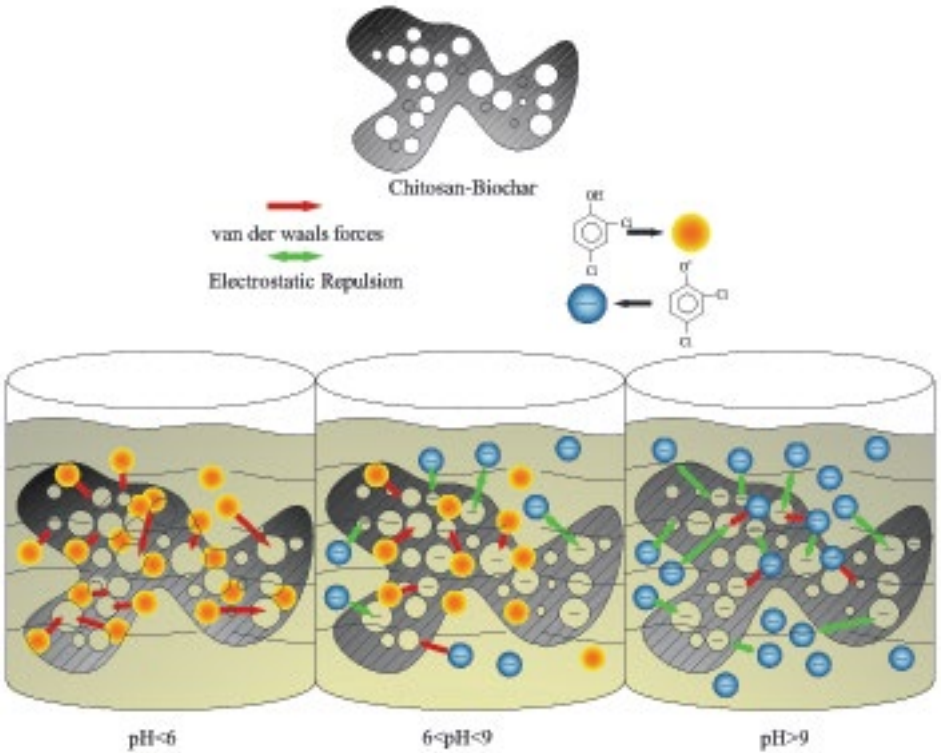

Fig. 8. Adsorption processes at different pH levels.

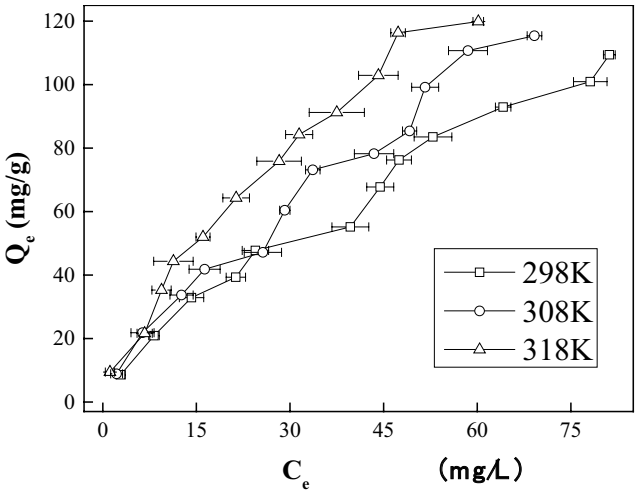

Fig. 9. Relationship between equilibrium concentration and adsorption capacity.

Table 1
Isotherm parameters for 2,4-DCP adsorption onto CBC

Model	Parameter	298 K	308 K	318 K
Freundlich	K_F	4.216	5.147	7.743
	$1/n$	0.682	0.735	0.739
	R^2	0.986	0.984	0.991
	SSE	9.465	8.146	12.165
Koble–Corrigan	A	4.578	5.654	5.245
	B	–0.001	–0.011	0.017
	n	0.712	0.767	0.899
	R^2	0.984	0.979	0.987
	SSE	16.973	25.568	16.579
Henry	A	12.665	11.623	17.121
	K	1.218	1.599	1.944
	R^2	0.988	0.978	0.981
	SSE	263.775	287.438	549.180

model tends to have a high correlation to adsorption processes in diluted solutions.

As shown in Fig. 12, the parameter A of the Henry model remained constant and the parameter K increased, as the temperature increased. The correlation coefficient R^2 exceeded 0.97, and the error value was negligible. The Henry model could describe the adsorption of 2,4-DCP on CBC.

In summary, all three models involved could describe the adsorption of 2,4-DCP on CBC. Based on the assumptions of the three models, it could be deduced that the adsorption of 2,4-DCP by CBC was a non-uniform surface one in a dilute solution.

3.3.2. Kinetics

As shown in Fig. 13, CBC had a fast adsorption effect for 2,4-DCP and the majority of 2,4-DCP was removed in the first 25 min, which was known as the rapid adsorption stage. At this stage, the removal rates of 2,4-DCP exceeded 75%. In 20–40 min, the removal rates increased slightly.

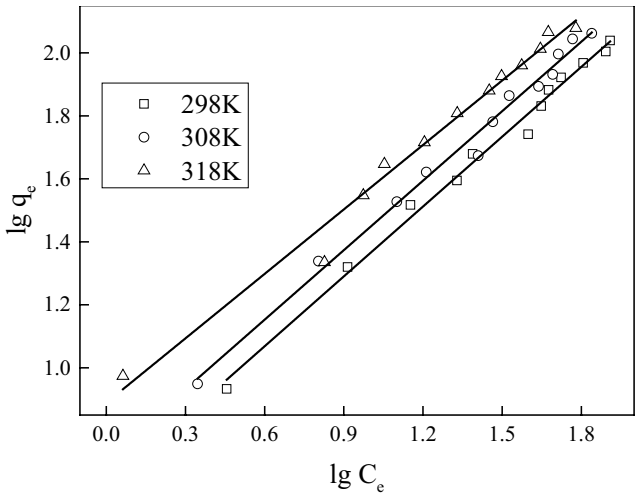

Fig. 10. Freundlich isotherm linear fitting.

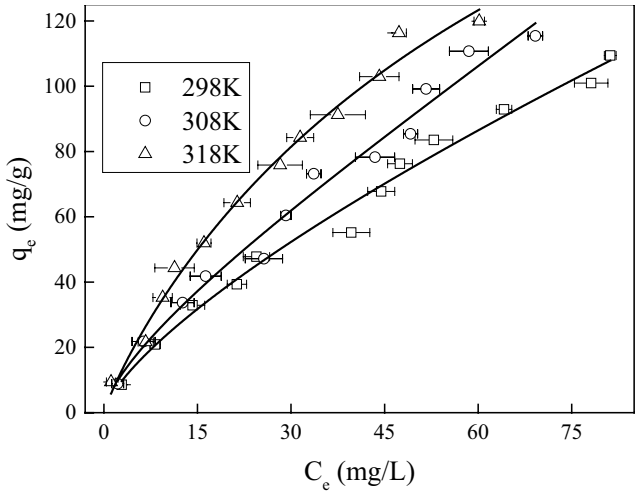

Fig. 11. Freundlich isotherm nonlinear fitting.

This stage was known as the slow adsorption stage. After that, adsorption equilibriums were reached and the removal rates remained constant.

The kinetic equation is mainly used to describe the adsorption rate. The adsorption mechanism can be inferred from the initial assumptions of the kinetic model. The adsorption of 2,4-DCP on CBC was discussed in the following two models.

The Elovich equation shows that the adsorption rate decreased exponentially as the adsorption capacity (or coverage) increased. Its integral form was expressed as [33]:

$$\frac{d_{Q_t}}{d_t} = \alpha e^{-\beta Q_t} \tag{8}$$

According to the boundary conditions (t = 0, Q_t = 0 and t = t, Q_t = Q_t), it is integrated as [34]:

$$Q_t = \frac{1}{\beta}\ln\left(t + t_0\right) - \frac{1}{\beta}\ln\left(t_0\right) \tag{9}$$

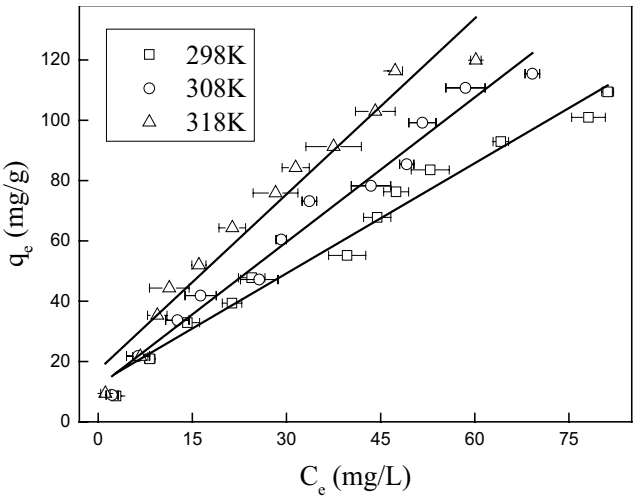

Fig. 12. Henry linear fitting.

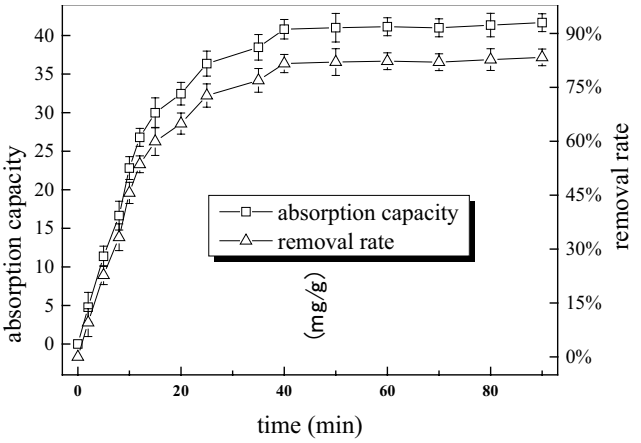

Fig. 13. Effect of time on 2,4-DCP removal.

where α (mg (g h)$^{-1}$) is the initial adsorption rate; β (g mg^{-1}) is a parameter related to surface coverage and activation energy; t_0 = 1/($\alpha\beta$); t(min) is the reaction time; Q_t(mg g^{-1}) is the adsorption degree at t.

The intraparticle diffusion (IPD) model is applied in the following form:

$$Q_t = R_d t^{\frac{1}{2}} \tag{10}$$

where R_d is the IPD rate constant (min^{-1}), Q_t is plotted against $t^{1/2}$ to get a straight line that is forced to pass through the origin; C is the intercept in the fitting equation. If C is close to 0, the IPD is the control step of the adsorption process; if C deviates significantly from 0, the IPD is not the only control step.

The parameters of the two model were evaluated and summarized in Table 2. As shown in Table 2 and Fig. 14, data fitted by the Elovich model had a high fitting degree, negligible error value, and good correlation. R^2 of the Elovich model exceeded 0.94. The IPD model was not suitable for adsorption of 2,4-DCP to CBC. The R^2 value was 0.79 and the

Table 2
Kinetic parameters for adsorption of 2,4-DCP to CBC

Parameter	Elovich model	IPD model
α	7.161	–
β	0.088	–
R_d	–	4.253
C		8.337
SSE(×10²)	0.115	4.065
R^2	0.942	0.789

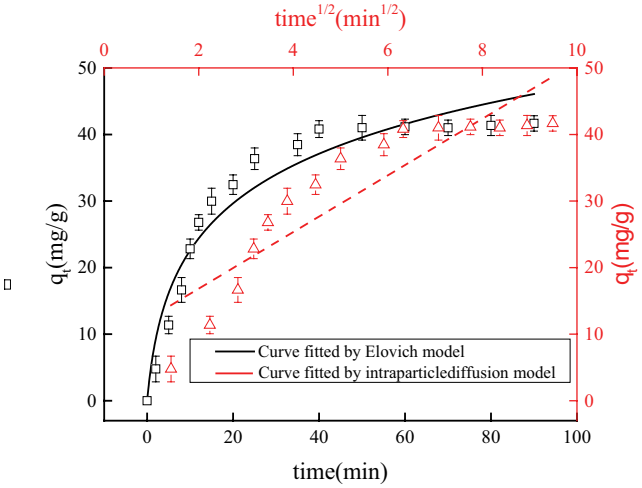

Fig. 14. Data fitting by the Elovich model and the IPD model.

C value was significantly different from 0, indicating that the adsorption process was also be affected by other mechanisms.

In order to further explore the adsorption mechanism, the adsorption phase and the equilibrium phase were segmentally fitted by the IPD model. The results are shown in Table 3 and Fig. 15. As observed, the adsorption phase and the equilibrium phase were quite different from each other. The intragranular diffusion rate constant in the adsorption phase (R_{d1}, >0.93) was significantly larger than that in the equilibrium phase (R_{d2}). The intercept in the adsorption phase (C_1 = –2.385) was significantly smaller than that in the equilibrium phase (C_2 = 39.331), indicating that the adsorption phase could be well fitted by the IPD model. However, the IPD model was not suitable for the equilibrium phase, where the adsorption process was controlled by other mechanisms.

In summary, the adsorption of 2,4-DCP on CBC was a physical adsorption process simultaneously controlled by surface diffusion and IPD. The mechanism was as follows: at the beginning, the adsorption process was dominated by surface diffusion and intra-ion diffusion; as the adsorption progresses, the adsorbates migrated from macropores to micropores through transition pores and the transfer rate gradually decreased in the inner pores. Meanwhile, the effects of IPD degraded gradually, while the effects of surface diffusion remained constant. Once the active sites in the inner pores of CBC were fully occupied, the IPD would no longer serve as a control step in adsorption. Once the active sites on the outer surface of CBC were fully occupied, the adsorption process reached a dynamic equilibrium and the adsorption capacity remained constant after that.

Table 3
IPD model parameters for two phases

Parameter	R_d	C	R^2
Adsorption phase	8.005	–2.385	0.9348
Equilibrium phase	0.229	39.331	0.742

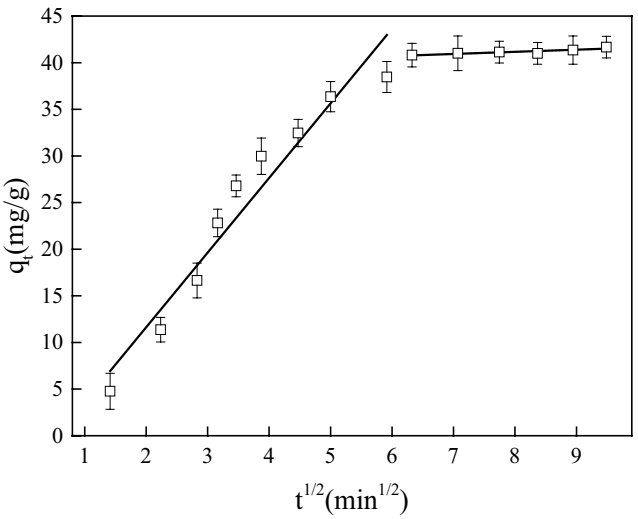

Fig. 15. Segmentally fitted curve of IPD model.

3.4. Effect of ionic strength and repeat performance

The effect of ionic strength on adsorption is complicated. In practical adsorption processes, the adsorption capacity may increase, decrease or remain unchanged as the ionic strength increased [35–38]. Ions are presented in all solutions and their effects on adsorption shall be investigated.

As shown in Fig. 16, the adsorption capacity per unit increased slightly (from 41.75 to 43.42 mg/g) as the concentration of Na^+ in the solution increased, suggesting that electrostatic interaction was not the primary control mechanism during this adsorption process.

Once being added to the 2,4-DCP solution, Na^+ competed for solvent molecules (H_2O), resulting in the migration of water molecules from 2,4-DCP molecules to Na^+. As a result, the solubility of 2,4-DCP and the hydrophilicity degraded. Upon addition of electrolyte to the solution, the solubility of solute was reduced. This phenomenon is known as salting-out [39]. The salting-out effect increased the contact possibility between 2,4-DCP molecules and CBC. As a result, adsorption of 2,4-DCP was favored due to increased hydrophobicity [40].

Under the optimal conditions, the biochar was leached with 70% ethanol several times for regenerate. Again, the recycled biochar was used to adsorb 2,4-DCP. It was found that the biochar could still maintain a removal rate of 41.2% after three cycles, and adsorption capacity was 20.6 mg/g.

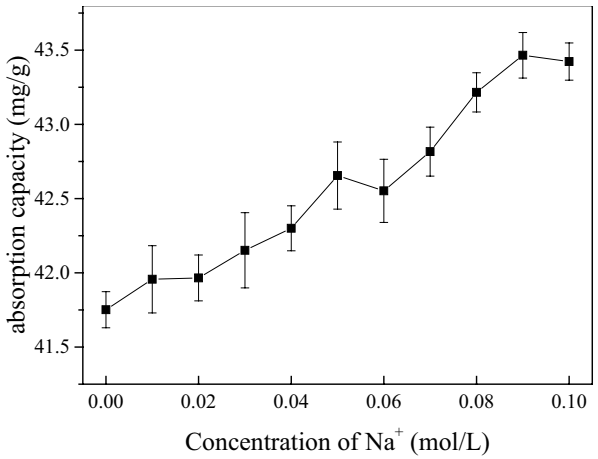

Fig. 16. Effect of ionic strength on 2,4-DCP removal.

4. Conclusions

In this study, biochar derived from chitosan was employed to remove 2,4-DCP. The optimized pH value for adsorption was 5.0. The optimized solution concentration of 2,4-DCP was 100 mg/L. For ensuring the adsorption equilibrium reached, the optimal adsorption time was 60 min. Considered both the energy consumption for heating and the fluctuation of the adsorption capacity at different temperatures, was room temperature considered to be the optimal adsorption temperature. Under the optimal conditions, was it found that the removal rate was 83.33%, and the absorption capacity was 41.65 mg/g. Investigations by FTIR indicated no changes of chemical bonds during adsorption. Investigations by SEM indicated that CBC was a bulky substance with a layered structure and branch-like extensions were commonly observed on biochar surfaces. Investigations by BET indicated that the adsorption process is typical physical adsorption on non-porous or macroporous adsorbents. All three isotherm models involved in this study (Freundlich, Koble–Corrigan, and Henry) could describe the adsorption process of 2,4-DCP on CBC. It could be deduced that the adsorption of 2,4-DCP by CBC was non-uniform surface adsorption in a diluted solution. Kinetics indicated that the adsorption rate at the rapid adsorption stage was simultaneously controlled by surface diffusion and IPD and that at the slow adsorption stage was controlled by surface diffusion. The ionic strengths suggested that electrostatic interaction was not the dominant mechanism during this process.

Acknowledgments

This work was supported by the National Natural Science Foundation of China (Grant No. 41571306), the Project of Excellent Fund in Hubei (Grant No. 2018CFA067), and the Major Project of Science and Technology Research Program of the Hubei Provincial Department of Education (Grant No. D20181101).

References

[1] B. Antizar-Ladislao, N.I. Galil, Biosorption of phenol and chlorophenols by acclimated residential biomass under bioremediation conditions in a sandy aquifer, Water Res., 38 (2004) 267–276.
[2] C. Su, R.W. Puls, Kinetics of trichloroethenereduction by zerovalent iron andtin: pretreatment effect, apparentactivation energy, and intermediateproducts, Environ. Sci. Technol., 33 (1999) 163–168.
[3] C.M. Hurdzan, R.P. Lanno, Determining exposure dose in soil: the effect of modifying factors on chlorinated benzene toxicity to earthworms, Chemosphere, 76 (2009) 946–951.
[4] Y. Wang, Y.P. Chen, Y.Z. Zhang, Investigation on the interaction of 2,4-dichlorophenol with human serum albumin, Chem. Bioeng., 28 (2011) 28–33.
[5] S. Asim, Y. Zhu, A. Batool, R. Hailili, J. Luo, Y. Wang, C. Wang, Electrochemical treatment of 2,4–dichlorophenol using a nanostructured 3D–porous Ti/Sb–SnO_2–Gr anode: reaction kinetics, mechanism, and continuous operation, Chemosphere, 185 (2017) 11–19.
[6] E. Sinirtas, M. Isleyen, G.S.P. Soylu, Photocatalytic degradation of 2,4-dichlorophenol with V_2O_5-TiO_2 catalysts: effect of catalyst support and surfactant additives, Chin. J. Catal., 37 (2016) 607–615.
[7] J. Wei, X. Xu, Y. Liu, D. Wang, Catalytic hydrodechlorination of 2,4-dichlorophenol over nanoscale Pd/Fe: reaction pathway and some experimental parameters, Water Res., 40 (2006) 348–354.
[8] A.S. Ghatbandhe, M.K. Yenkie, 2,4 dichlorophenol (2,4-DCP) sorption from aqueous solution using granular activated carbon and polymeric adsorbents and studies on effect of temperature on activated carbon adsorption, J. Environ. Sci. Eng., 50 (2008) 163–168.
[9] A. Hass, J.M. Gonzalez, I.M. Lima, H.W. Godwin, J.J. Halvorson, D.G. Boyer, Chicken manure biochar as liming and nutrient source for acid Appalachian soil, J. Environ. Qual., 41 (2012) 1096–1106.
[10] Z. Wang, H. Guo, F. Shen, G. Yang, Y. Zhang, Y. Zeng, L. Wang, H. Xiao, S. Deng, Biochar produced from oak sawdust by Lanthanum (La)-involved pyrolysis for adsorption of ammonium (NH_4^+), nitrate (NO_3^-), and phosphate (PO_4^{3-}), Chemosphere, 119 (2015) 646–653.
[11] M.K. Hossain, V. Strezov, K.Y. Chan, A. Ziolkowski, P.F. Nelson, Influence of pyrolysis temperature on production and nutrient properties of wastewater sludge biochar, J. Environ. Manage., 92 (2011) 223–228.
[12] K.G. Roberts, B.A. Gloy, S. Joseph, N.R. Scott, J. Lehmann, Life cycle assessment of biochar systems: estimating the energetic, economic, and climate change potential, Environ. Sci. Technol., 44 (2010) 827–833.
[13] M.J. Antal, M. Grønli, The art, science, and technology of charcoal production, Ind. Eng. Chem. Res., 42 (2003) 1619–1640.
[14] S. Zhang, H. Gao, J. Li, Y. Huang, A. Alsaedi, T. Hayat, X. Xu, X. Wang, Rice husks as a sustainable silica source for hierarchical flower-like metal silicate architectures assembled into ultrathin nanosheets for adsorption and catalysis, J. Hazard. Mater, 321 (2017) 92–102.
[15] X. Liu, J. Li, X. Wang, C. Chen, X. Wang, High performance of phosphate-functionalized graphene oxide for the selective adsorption of U(VI) from acidic solution, J. Nucl. Mater., 466 (2015) 56–64.
[16] X. Liu, J. Wu, S.W. Zhang, C.C. Ding, G.D. Sheng, A. Alsaedi, T. Hayat, J.X. Li, Y.T. Song, Amidoxime-functionalized hollow carbon spheres for efficient removal of uranium from wastewater, ACS Sustainable Chem. Eng., 7 (2019) 10800–10807.
[17] G. Li, W. Zhu, L. Zhu, X. Chai, Effect of pyrolytic temperature on the adsorptive removal of P-benzoquinone, Korean J. Chem. Eng., 33 (2016) 2215–2221.
[18] Z. Qiying, J. Xia, L. Xi, J.C. Qiang, J. Wenju, Preparation of high-yield N-doped biochar from nitrogen-containing phosphate and its effective adsorption for toluene, RSC Adv., 8 (2018) 30171–30179.
[19] H. Xu, X. Zhang, Y. Zhang, Modification of biochar by Fe_2O_3 for the removal of pyridine and quinoline, Environ. Technol., 39 (2018) 1470–1480.
[20] J. Sun, X. Liu, F. Zhang, J. Zhou, J. Wu, A. Alsaedi, T. Hayat, J. Li, Insight into the mechanism of adsorption of phenol

and resorcinol on activated carbons with different oxidation degrees, Colloids Surf., A, 563 (2019) 22–30.
[21] S.Y. Oh, Y.D. Seo, K.S. Ryu, D.J. Park, S.H. Lee, Redox and catalytic properties of biochar-coated zero-valent iron for the removal of nitro explosives and halogenated phenols, Environ. Sci. Processes Impacts, 19 (2017) 711–719.
[22] M. Rinaudo, Chitin and chitosan: properties and applications, Prog. Polym. Sci., 31 (2006) 603–632.
[23] S. Sugashini, K.M.M.S. Begum, Performance of ozone treated rice husk carbon (OTRHC) for continuous adsorption of Cr(VI) ions from synthetic effluent, J. Environ. Chem. Eng., 1 (2013) 79–85.
[24] T. Pal, T. Kar, Single crystal growth and characterization of the nonlinearoptical crystal L-arginine hydrofluoride, J. Cryst. Growth, 234 (2002) 267–271.
[25] J. Wu, D. Ren, X. Zhanga, Z. Chen, S. Zhang, S. Li, L. Fu, The adsorption properties of biochar derived from woody plants or bamboo for cadmium in aqueous solution, Desal. Water Treat., 160 (2019) 268–275.
[26] R.G. Tobin, S. Chiang, P.A. Thiel, P.L. Richards, The C=O stretching vibration of CO on Ni(100) by infrared emission spectroscopy, Surf. Sci., 140 (1984) 393–399.
[27] L. Feng, X.P. Ge, D.S. Wang, H.X. Tang, Effects of pH value on the adsorption and degradation of 2,4-DCP by nanoscale zero-valent iron, Environ. Sci., 33 (2012) 94–103.
[28] K.M. Ponvel, D. Kavitha, K.-M. Kim, C.-H. Lee, Adsorption of 2,4-dichlorophenol on metal-nitrate modified activated carbon, Korean J. Chem. Eng., 26 (2009) 1379–1382.
[29] Q. Luo, X. Zhang, H. Wang, Y. Qian, Mobilization of phenol and dichlorophenol in unsaturated soils by non-uniform electrokinetics, Chemosphere, 59 (2005) 1289–1298.
[30] I. Langmuir, The constitution and fundamental properties of solids and liquids, J. Franklin Inst., 183 (1917).
[31] K.G. Bhattacharyya, S.S. Gupta, Removal of Cu(II) by natural and acid-activated clays: an insight of adsorption isotherm, kinetic and thermodynamics, Desalination, 272 (2011) 66–75.
[32] S. Gupta, B.V. Babu, Removal of toxic metal Cr(VI) from aqueous solutions using sawdust as adsorbent: equilibrium, kinetics and regeneration studies, Chem. Eng. J., 150 (2009) 352–365.
[33] C.W. Cheung, J.F. Porter, G. Mckay, Sorption kinetics for the removal of copper and zinc from effluents using bone char, Sep. Purif. Technol., 19 (2000) 55–64.
[34] M.S. El-Shahawi, H.A. Nassif, Retention and thermodynamic characteristics of mercury(II) complexes onto polyurethane foams, Anal. Chim. Acta, 481 (2003) 29–39.
[35] J. Lützenkirchen, Ionic strength effects on cation sorption to oxides: macroscopic observations and their significance in microscopic interpretation, J. Colloid Interface Sci., 195 (1997) 149–155.
[36] Z. Wu, J. Wu, H. Xiang, M.-S. Chun, K. Lee, Organosilane-functionalized Fe_3O_4 composite particles as effective magnetic assisted adsorbents, Colloids Surf., A, 279 (2006) 167–174.
[37] L. You, Z. Wu, T. Kim, K. Lee, Kinetics and thermodynamics of bromophenol blue adsorption by a mesoporous hybrid gel derived from tetraethoxysilane and bis(trimethoxysilyl)hexane, J. Colloid Interface Sci., 300 (2006) 526–535.
[38] X. Ye, T. Liu, Q. Li, H. Liu, Z. Wu, Comparison of strontium and calcium adsorption onto composite magnetic particles derived from Fe_3O_4 and bis(trimethoxysilylpropyl)amine, Colloids Surf., A, 330 (2008) 21–27.
[39] P.K. Grover, R.L. Ryall, Critical appraisal of salting-out and its implications for chemical and biological sciences, Chem. Rev., 105 (2005) 1–10.
[40] J.P. Chen, S. Wu, Simultaneous adsorption of copper ions and humic acid onto an activated carbon, J. Colloid Interface Sci., 280 (2004) 334–342.